buildings

MDPI

Article

Application and Optimization of Reinforced Concrete Noise Barrier

Milica Jovanoska-Mitrevska [1], Todorka Samardzioska [1] and Slobodan B. Mickovski [2,*]

[1] Faculty of Civil Engineering, Ss. Cyril and Methodius University in Skopje, 1000 Skopje, North Macedonia; m.jovanoska@gf.ukim.edu.mk (M.J.-M.); samardzioska@gf.ukim.edu.mk (T.S.)
[2] Built Environment Asset Management Centre, Glasgow Caledonian University, Glasgow G4 0BA, Scotland, UK
* Correspondence: slobodan.mickovski@gcu.ac.uk

Abstract

Urbanization and increased traffic across Europe are leading to increased exposure of the population to harmful levels of noise, primarily caused by road traffic. Over 30% of the population is exposed to levels exceeding the limits recommended by the World Health Organization (WHO). Among the various noise reduction strategies, reinforced concrete noise barriers stand out as one of the most effective passive measures. This research analyses the geometric optimization of reinforced concrete noise barriers with different top-edge designs (flat, T-shape, symmetric and asymmetric V-shape) using the Bound Optimization by Quadratic Approximation (BOBYQA) method. The analysis was conducted using COMSOL Multiphysics software, where a coupled solid mechanics and pressure acoustics model was developed. The simulations were performed in a frequency range from 50 to 3150 Hz. The results show that geometry has a significant impact on acoustic efficiency, with the asymmetric V-shape demonstrating the greatest noise reduction. These findings highlight the key role of geometric optimization in the design of cost-effective and sustainable noise protection solutions.

Keywords: noise; reinforced concrete barriers; traffic noise; geometric optimization; finite element method; COMSOL multiphysics software

1. Introduction

Across Europe, growing cities and increased road traffic have raised community exposure to environmental noise, with road traffic being the main source. According to a report by the European Environment Agency in 2025, one in five Europeans live in an environment where noise limits are exceeded [1]. Under the more stringent guidelines of the World Health Organization (WHO), this percentage exceeds 30% of the population, indicating a high prevalence of chronic exposure to harmful noise levels. Road traffic is identified as the most widespread source of noise, exposing over 92 million people to levels above the day–evening–night sound level (L_{den}) reporting threshold of 55 dB used under the European Union Environmental Noise Directive (EU END) [1,2].

Noise not only affects quality of life but also has significant public health consequences. Research links chronic noise exposure to an increased risk of cardiovascular disease, premature mortality, sleep disorders, diabetes, cognitive impairment in children, and behavioral problems [3,4]. Additionally, noise pollution also has a negative impact on ecosystems (terrestrial and aquatic), contributing to a decrease in biodiversity [5,6].

Check for updates

Academic Editor: Salvatore Verre

Received: 1 December 2025
Revised: 31 January 2026
Accepted: 10 February 2026
Published: 12 February 2026

Copyright: © 2026 by the authors. Licensee MDPI, Basel, Switzerland. This article is an open access article distributed under the terms and conditions of the Creative Commons Attribution (CC BY) license.

In contemporary traffic noise control practice, noise barriers (NBs) are widely applied as an effective passive mitigation measure. In addition to them, other methods are also applied, such as controlling the type and number of vehicles, speed limits, use of quiet road surfaces, technological advances in vehicle design and engines with reduced noise, as well as appropriate land use planning and spatial planning in zones. Noise barriers are most commonly installed along highways, city streets, railways, industrial complexes and airports, but also near environmentally sensitive zones where special noise protection is required. Improving the acoustic efficiency of noise barriers represents a direct and effective means of reducing population exposure to traffic noise, thereby contributing to measurable public health benefits and mitigating adverse ecological impacts.

Noise barriers are usually constructed using a range of different materials, depending on the purpose and location of installation. They can be transparent, such as polycarbonate or glass, which allow for visibility and do not obstruct the view. Metal, wooden or reinforced concrete barriers are also used, which are known for their durability and effective noise protection. In addition, natural and vegetative barriers, such as earthen embankments and planted green areas, represent a significant alternative that, in addition to reducing sound, also contribute to improving the esthetic and ecological quality of a space. According to the technical report of the Conference of European Directors of Roads (CEDR) [7], the usual height of noise barriers in Europe ranges from 2 to 5 m, with the minimum permitted height being from 1 to 2.5 m, and the maximum can reach over 10 m.

The functional principles and mechanisms of noise barriers are shown in Figure 1. The noise barrier interrupts the direct path of sound from the source to the receiver. Part of the sound energy that encounters the barrier is reflected back to the source, the barrier material absorbs another part, and the remaining part is transmitted to the other side. In addition to the transmitted sound, the receiver also receives a portion of the sound waves that undergo diffraction from the top of the barrier. The transmission of sound depends on the material properties of the barrier and its thickness, and the diffraction on its shape, dimensions, and placement in space [7].

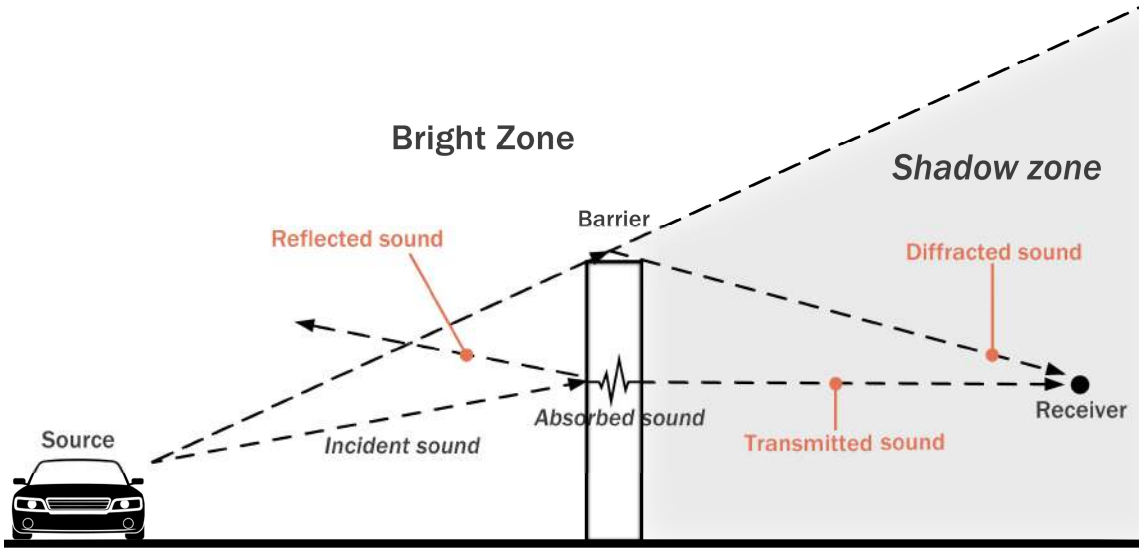


Figure 1. Sound transmission mechanisms in noise barriers, adapted from [7].

With progressing urbanization, optimizing noise barriers is becoming increasingly important in order to effectively deal with protecting the environment within the confines of limited space. In addition, modern trends in sustainable development impose the need to reduce the amount of materials used, from an economic point of view, as well as from the

aspect of reducing CO_2 emissions and sustainability in general. Accordingly, improving noise barrier performance without increasing structural dimensions is a key objective.

Numerous studies have investigated the acoustic performance of rigid noise barriers with modified top-edge geometries. Fard et al. [8] employed the finite element method (FEM) to evaluate vertical, inclined and wedge-shaped barriers, as well as barriers with arrow-shaped, T-shaped and V-shaped barrier edges. Sun et al. [9] analyzed T-shaped and Y-shaped barriers using empirical formulations. Monazzam et al. [10] assessed the performance of T-shaped barriers incorporating oblique diffusers using the boundary element method (BEM). Wang et al. [11] studied barriers equipped with different types of wells at the top edge using the BEM. Komkina et al. [12] conducted FEM simulations to compare vertical and T-profile barrier designs.

Beyond performance evaluation, several studies have addressed the optimization of top-edge geometries to enhance acoustic shielding without significantly increasing barrier height. Bugaru et al. [13] optimized an inclined Y-shaped barrier edge while accounting for ground absorption-reflections and atmospheric absorption, using a combination of analytical and semi-empirical noise prediction methodologies. Liu et al. [14] applied an isogeometric singular boundary method to the shape optimization of Y-shaped and T-shaped barriers. Toledo et al. [15] conducted multi-objective optimization of various barrier geometries, including polygonal, spline-based, Y-shaped, tree-shaped and fork-shaped designs, with the simultaneous goals of maximizing noise attenuation and minimizing material usage. They used the two-dimensional dual boundary element method combined with evolutionary multi-objective optimization.

These studies generally indicate that rigid top-edge modifications are particularly effective at medium and high frequencies, as short wavelengths are not as easily diffracted into the shadow zone.

To improve barrier performance, including the lower frequencies, many researchers have introduced sound-absorbing materials into barrier designs. Such treatments reduce reflected sound energy and mitigate multiple reflections between the barrier and nearby surfaces. Ishizuka et al. [16] investigated barriers with various edge shapes and acoustical conditions using the BEM, including vertical and T-shaped barriers, as well as configurations with cylindrical, double-cylindrical, branched, and multi-edged terminations. Grubeša et al. [17] combined the BEM and genetic algorithms to optimize T-shaped barriers with absorptive treatments. Costa et al. [18] employed fundamental solutions to predict the acoustic performance of absorptive T-shaped thin barriers. Liu et al. [19] conducted performance analysis and material distribution optimization of sound-absorbing materials on the surface of a vertical noise barrier, a half-Y-shaped noise barrier and a T-shaped noise barrier using a semianalytical meshless method. Jolibois [20] performed numerical optimization of rigid and absorptive barriers using a gradient-based approach coupled with BEM, and Liu et al. [21] optimized porous material thickness on noise barriers using meshless techniques.

More recent developments include active noise control concepts integrated with noise barriers to address the low-frequency limitations of purely passive designs [22,23], as well as metamaterial-based barrier concepts aimed at achieving enhanced attenuation within a targeted frequency range [24,25].

Reinforced concrete noise barriers are one of the most commonly used solutions due to their durability and structural performance. An effective approach to improving their acoustic efficiency, without increasing barrier height, is the application of optimized top-edge terminations. Despite extensive research on vertical, T-shaped, and V-shaped barrier tops, non-symmetrical V-shaped top-edge geometries have received limited attention.

Therefore, the objective of this study is to numerically investigate and optimize reinforced concrete noise barriers with different top-edge geometries, including standard vertical, T-shaped, V-shaped and non-symmetrical V-shaped configurations, with the aim of reducing traffic noise-related health and environmental impacts. The acoustic performance of these designs is evaluated and compared in order to assess the potential of non-symmetrical V-shaped terminations for improving noise barrier efficiency with minimal additional material usage.

2. Materials and Methods

2.1. Model Data

This study considers reinforced concrete noise barriers with and without top-edges. As a practical design reference, guidance from the Noise Barrier Design Handbook of the Federal Highway Administration (FHWA) was consulted. The handbook indicates that typical minimum thicknesses are approximately 125 mm for precast concrete noise barriers and 150–200 mm for cast-in-place reinforced concrete barriers [26]. A thickness of 150 mm was adopted for this research.

The analysis covers five types of noise barriers (Figures 2–5):

- NB1: Noise barrier, height H = 3 m, without a top edge.
- NB2: Noise barrier, height H = 3 m + symmetrical T-shape edge with length B.
- NB3: Noise barrier, height H = 3 m + symmetrical V-shape edge with length B.
- NB4: Noise barrier, height H = 3 m + asymmetrical V-shape edge with length B.
- NB5: Noise barrier without top-edge, but with an increased height of H = 4.4 m, achieving an equivalent volume to barriers NB3 and NB4 and approximately to NB2.

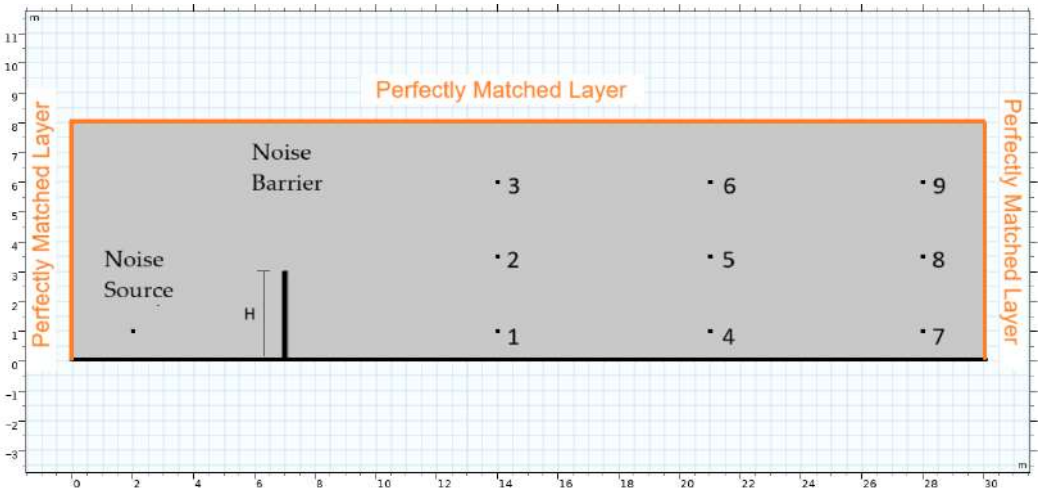


Figure 2. Reinforced concrete noise barrier, NB1, with height H = 3 m.

The width of the B top edge is optimized based on the model of the barrier NB2 and the same is adopted for NB3 and NB4. The sound source is modeled as a point and is placed at a distance of 5 m from the noise barrier in order to simulate the average distance of vehicles on a highway [10]. The height of the source is 1 m above ground level, which corresponds to the height of a vehicle engine. The receiving points are arranged in a regular grid, at horizontal distances of 7 m, 14 m and 21 m from the noise barrier and at vertical distances of 1 m, 3.5 m and 6 m from ground level. In this way, exposure of single-story and two-story buildings near road infrastructure was simulated. The geometry of the models is given in Figures 2–5.

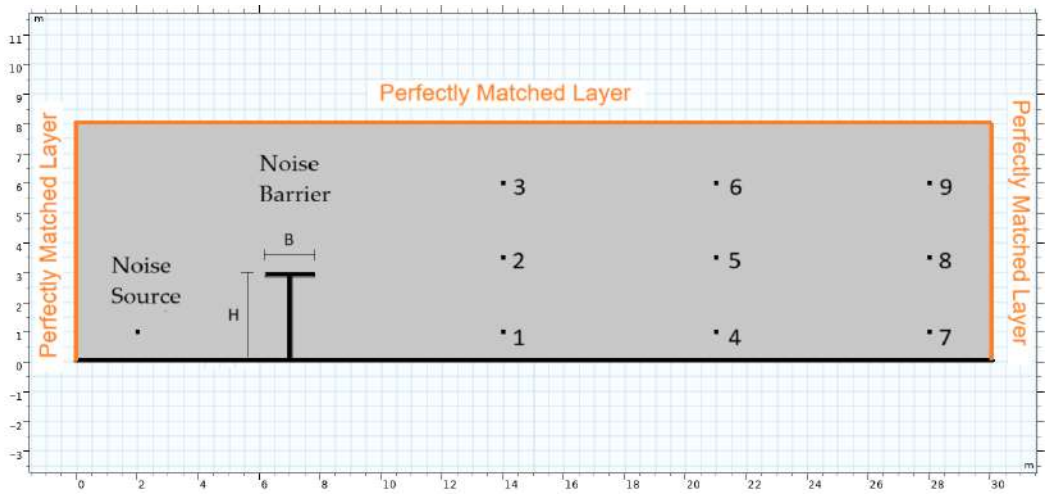


Figure 3. Reinforced concrete noise barrier, NB2, with height H = 3 m, with symmetrical T top edge and width B.

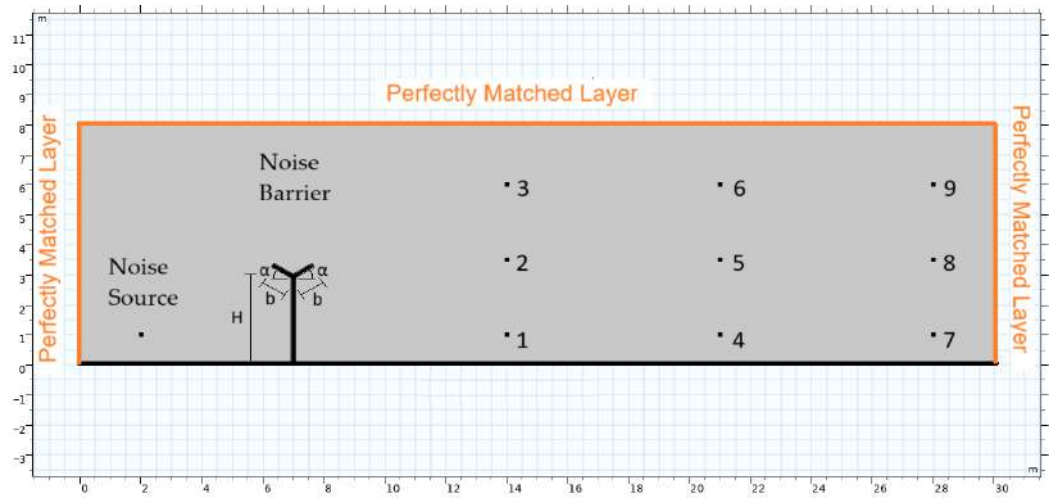


Figure 4. Reinforced concrete noise barrier, NB3, with height H = 3 m, with symmetrical V top edge and width $B = 2b$.

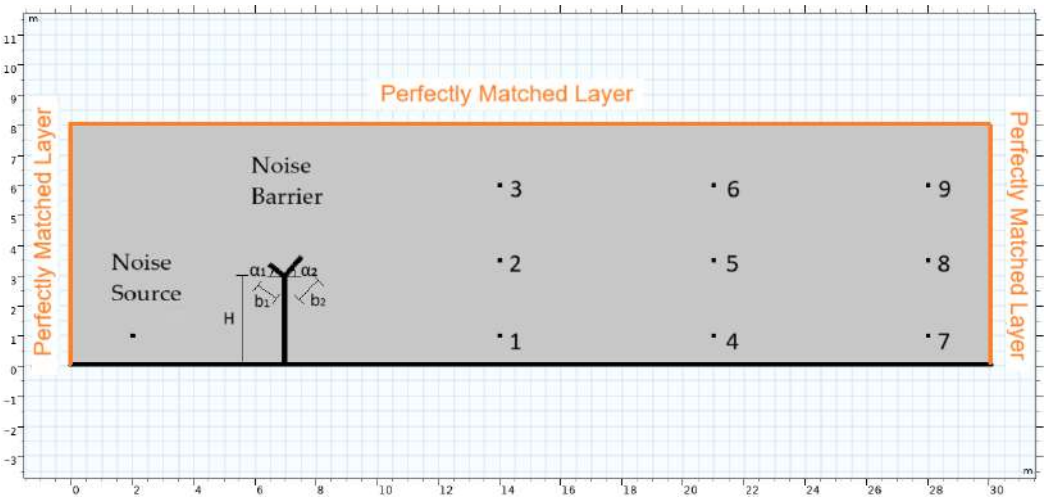


Figure 5. Reinforced concrete noise barrier, NB4, with height H = 3 m, with asymmetrical V top edge and width $B = b_1 + b_2$.

2.2. Numerical Calculation

The numerical calculation was performed using the finite element method with the COMSOL Multiphysics software V6.0. Two modules (physics interfaces) were coupled: a module for solid mechanics and a module for the propagation of sound waves in air (pressure acoustics). The calculation was performed in the frequency domain for the central frequencies of the 1:3 octave spectrum from 100 Hz to 3150 Hz.

To maintain computational feasibility while resolving the acoustic field over the full frequency set, the model was formulated in two dimensions (2D). In a 2D acoustic formulation, the sound field is assumed to be invariant in the out-of-plane direction, which corresponds to the idealization of an infinitely long barrier and a line source. This representation captures the dominant sound propagation and diffraction mechanisms in the vertical plane perpendicular to the barrier and is commonly adopted for comparative studies of barrier edge modifications. Under these assumptions, the 2D model resolves the primary top-edge diffraction effects for long, straight barriers, with a substantially reduced computational cost relative to fully three-dimensional simulations.

The noise barrier was modeled within the solid mechanics module, and everything else was modelled within the pressure acoustics module.

For the solid domain, the solid mechanics interface in COMSOL Multiphysics was used to model the frequency domain structural response, governed by the following:

$$-\rho_s\omega 2\mathbf{u} = \nabla\cdot\boldsymbol{\sigma} + \mathbf{F}_v \quad (1)$$

where $\boldsymbol{u}$ is the displacement vector, ρ_s is the material density, ω is the angular frequency, $\boldsymbol{\sigma}$ is the Cauchy stress tensor, and $\boldsymbol{F_v}$ represents body (volume) force.

The pressure acoustics–frequency domain interface in COMSOL Multiphysics solves the Helmholtz equation:

$$\nabla\cdot(-1/\rho_f\,(\nabla p - \mathbf{q_d})) - \omega\hat{}2/(\rho_fc\hat{}2)\,p = Q_m \quad (2)$$

where p is the acoustic pressure, ρ_f is the density of the fluid medium, c is the speed of sound, ω is the angular frequency, $\boldsymbol{q_d}$ represents a dipole source, and Q_m denotes a monopole source term.

The sound source in this case was modeled as a point source with a given pressure of $p_0 = 1$ Pa (Dirichlet condition, $q_d = 0$, $Q_m = 0$), which is equivalent to a sound level of approximately 94 dB. In a two-dimensional acoustic formulation, a point pressure excitation represents an infinitely long line source perpendicular to the modeling plane.

Two physical conditions were imposed on the boundary between the noise barrier and the air. The boundary load F set on the solid is as follows:

$$F = -\mathbf{n_s}\,p \quad (3)$$

where n_s is the outward-pointing unit normal vector seen from inside the solid domain. Furthermore, on the fluid side, the normal acceleration experienced by the fluid is set equal to the normal acceleration of the solid:

$$-\mathbf{n_a}\cdot(-1/\rho_f\,\nabla p) = a_n \quad (4)$$

where $\boldsymbol{n_a}$ is the outward-pointing unit normal vector seen from inside the acoustics domain and a_n is the normal acceleration and it is set to $(\boldsymbol{n_a}\cdot\cdot\cdot\boldsymbol{u})\,\omega^2$ [27].

The air domain was modeled as rectangle with dimensions of 30 m × 8 m. To simulate the infinity of the air domain, without distorting the sound field, perfectly matched layers

(PMLs) were applied along the contours of the air domain, with the exception of the lower contour, where an impedance boundary condition was set through the sound absorption coefficients of asphalt. In the frequency domain, the PML is implemented through a complex-valued coordinate transformation that introduces an absorbing behavior with maintained wave impedance, eliminating reflections at the interface [28].

The largest element of the finite element free triangular mesh was limited by the highest calculation frequency, i.e., one sixth of its wavelength, $a_{max} = \lambda_{max}/6 = 343/3150/6 = 0.018$ m. The total number of mesh elements was 2,049,566 for NB1, 2,051,540 for NB2, 2,050,316 for NB3, 2,050,456 for NB4 and 2,044,768 for NB5. The corresponding total numbers of degrees of freedom were 4,192,837 for NB1, 4,199,257 for NB2, 4,199,474 for NB3, 4,199,697 for NB4 and 4,187,091 for NB5.

2.3. Materials

Within the numerical model, it was necessary to define the material properties of the noise barrier, the air domain and the asphalt substrate.

The material model for the reinforced concrete noise barrier is linearly elastic, with the properties given in Table 1.

Table 1. Properties of reinforced concrete (solid mechanics module).

Density [kg/m^3]	2500
Young's Module of Elasticity [GPa]	30
Poisson ratio	0.22

For the air domain, the standard acoustic properties of air within the sound wave transmission module were used, as presented in Table 2.

Table 2. Air properties (pressure acoustics module).

Density [kg/m^3]	1.2044
Speed of sound in air [m/s]	343

The asphalt is modeled with an impedance boundary condition within the sound wave transmission module. For this purpose, the absorption coefficients for the asphalt at different frequencies are required, as shown in Table 3.

Table 3. Properties of asphalt (pressure acoustics module).

f [Hz]	**α**
125	0.03
250	0.05
500	0.1
1000	0.12
2000	0.15
5000	0.2

2.4. Optimization

Model optimization was performed in COMSOL Multiphysics using the Bound Optimization BY Quadratic Approximation (BOBYQA) algorithm, a derivative-free, local optimization method. BOBYQA constructs a quadratic approximation of the objective

function that is valid within the region around the current iterate, the so-called trust region. The quadratic model is iteratively updated by minimizing the Frobenius norm of the difference between the Hessians of successive quadratic models [29]. As a derivative-free, bound-constrained optimizer, BOBYQA is well suited to problems with a small number of design variables and costly model evaluations, such as the present study.

The objective of the optimization was the minimization of the mean sound pressure level (dB) evaluated at nine fixed receiver positions and aggregated over the frequency set F:

$$J = \sum_{f \in F} \langle L_p(f) \rangle \tag{5}$$

where J denotes the objective function, $\langle L_p\ (f) \rangle$ is the average value of the sound pressure level at the nine fixed receiver positions, and F is the set of one-third octave band center frequencies spanning 100–3150 Hz.

The optimization was carried out over the entire defined frequency range within the parameter bounds listed in Table 4. The bounds on the top-edge length B were defined based on practical construction considerations, while the edge slope was limited to 80° in order to ensure an inclined edge configuration. The optimization procedure was repeated from multiple initial guesses within the admissible bounds of B and α in order to reduce sensitivity to the starting point and the risk of convergence to suboptimal local minima. The Efficient Global Optimization (EGO) algorithm was additionally used as a verification check to assess whether a better solution could be identified within the same parameter bounds; no improvement over the locally optimized solutions was obtained.

Table 4. Limits of variables in the process of optimization.

Length of Top Edge B, Where $b_1 + b_2 = 2b = B$		**Edge Slopes, α, α_1, α_2**	
Lower Limit	**Upper Limit**	**Lower Limit**	**Upper Limit**
0.35 [m]	2 [m]	0 [°C]	80 [°C]

The optimality tolerance was set to 0.001, and the maximum number of model evaluations was limited to 1000. Constraint handling was performed using an augmented Lagrangian approach.

2.5. Numerical Experiment Workflow

For clarity and reproducibility, the stages of the numerical experiment performed in this study are summarized below as an algorithmic procedure and are illustrated in Figure 6.

The steps of the numerical procedure are explained in more detail below.

- Geometry creation: The two-dimensional barrier geometry (NB1–NB5) and the surrounding air domain, together with the source and receiver points, are created in COMSOL Multiphysics.
- Material assignment: Material properties are assigned to each domain (reinforced concrete for the barrier, air for the air domain and asphalt ground modeled via absorption data).
- Physics interfaces: The solid mechanics interface is applied to the barrier domain and the pressure acoustics interface is applied to the air domain.
- Source definition: The sound source is defined as a point pressure p_0 = 1 Pa (Dirichlet boundary condition) at the specified source location.

- Boundary conditions: Acoustic–structure interaction conditions are applied at the barrier–air interface; an impedance boundary condition is applied at the ground; and perfectly matched layers (PMLs) are applied at the outer boundaries of the air domain.
- Meshing: A free triangular mesh is generated with maximum element size constrained by the highest analyzed frequency (element size limited to one-sixth of the minimum wavelength).
- Frequency domain analysis: Simulations are performed for the 1/3 octave band center frequencies from 100 Hz to 3150 Hz.
- Objective function formulation and evaluation: Sound pressure levels are extracted at the predefined receiver points, and the objective function is computed as the average sound pressure level over all receiver points.
- Optimization: Selected top-edge geometric parameters (within the prescribed bounds) are optimized using the BOBYQA algorithm to minimize the objective function.
- Post-processing and comparison: The sound pressure levels at all receiver points are evaluated and the barrier configurations are compared based on the resulting acoustic performance.

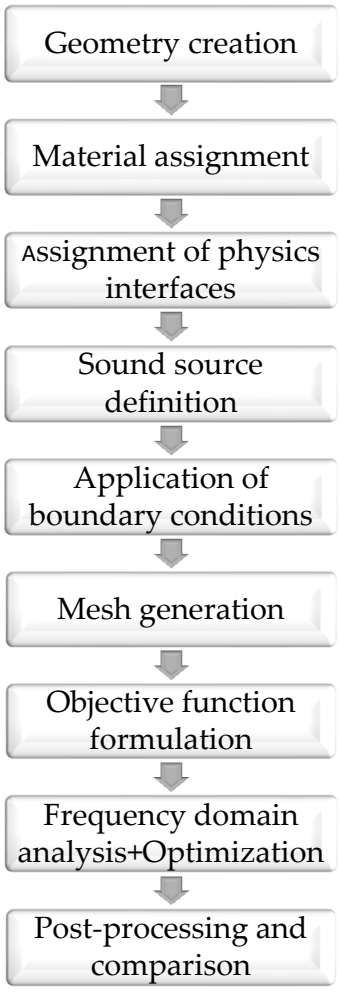


Figure 6. Numerical experiment workflow implemented in COMSOL Multiphysics.

3. Results and Discussion

After the optimization process, the optimal geometric parameters and the corresponding values of the minimized objective function were obtained and are summarized in

Table 5. The reference barriers NB1 and NB5 are also included in the table for comparison. The corresponding noise barrier geometries are illustrated in Figure 7.

Table 5. Optimized geometric parameters of NB2–NB4 and corresponding values of the objective function, with reference vertical noise barriers, NB1 and NB5, included for comparison.

Barrier	Length of Top Edge $B = 2b = b_1 + b_2$	Edge Slope	Objective Function (Sum of the Average Sound Levels at 9 Reception Points for All Frequencies)
NB1	–	–	687.8 dB
NB2	B = 1.616 m	–	653 dB—minimized
NB3	B = 0.808 m	$\alpha = 47.9°$	616.7 dB—minimized
NB4	b_1 = 0.78 m, b_2 = 0.836 m	$\alpha_1 = 47.7°$, $\alpha_2 = 60.6°$	604.3 dB (609.4 dB with negative values eliminated)—minimized
NB5	–	–	641.7 dB

Note: "–" indicates that the parameter is not applicable for the given barrier configuration.

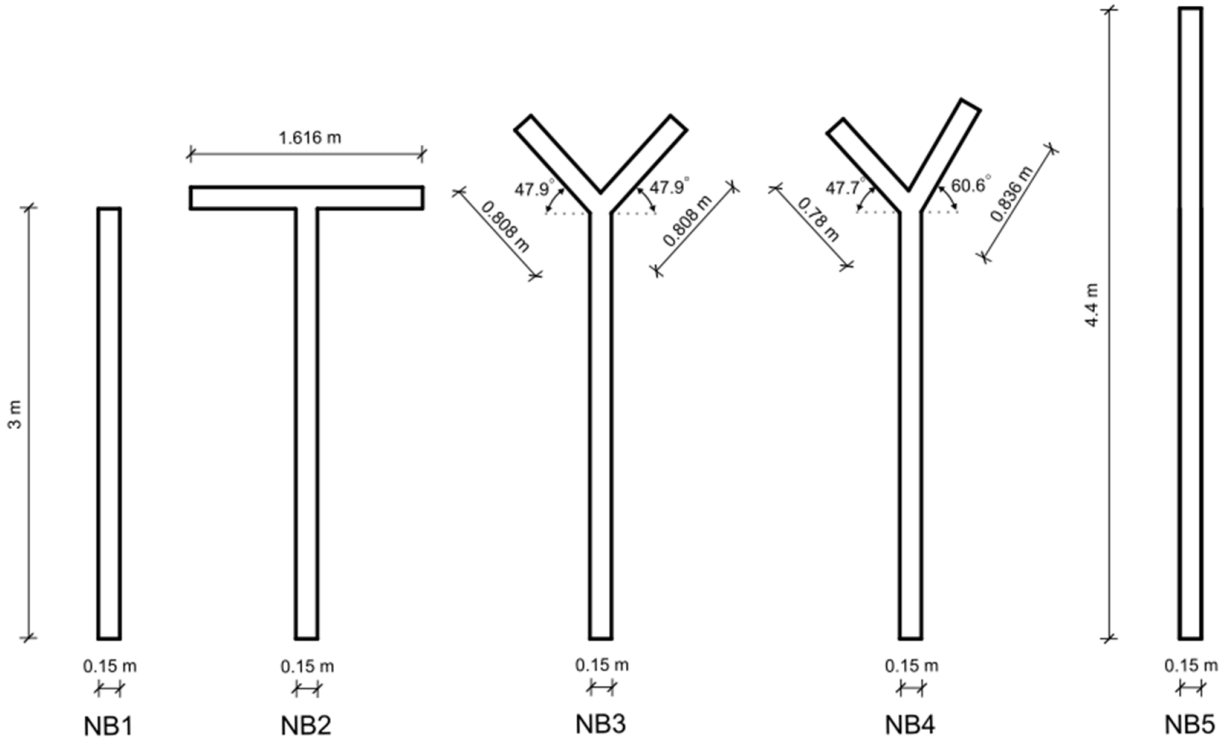


Figure 7. Geometrical representation of the reference vertical noise barrier without a top edge (NB1), the optimized noise barrier configurations with top edges (NB2–NB4), and a vertical noise barrier with volume equivalent to that of NB2–NB4 (NB5).

The sound level in dB by frequency was calculated for the optimized models. The calculation was made for a total of 16 frequencies—the central frequencies of the 1:3 octave spectrum: 100 Hz, 125 Hz, 160 Hz, 200 Hz, 250 Hz, 315 Hz, 400 Hz, 500 Hz, 630 Hz, 800 Hz, 1000 Hz, 1250 Hz, 1600 Hz, 2000 Hz, 2500 Hz and 3150 Hz. Figures 8–12 provide a graphical representation of the sound level for the frequency 125 Hz for all barriers, while Figures 13–17 provide a graphical representation of the sound level for the frequency 1250 Hz.

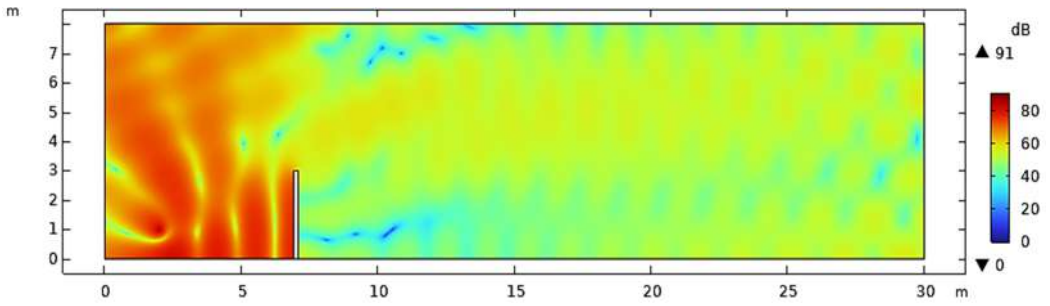


Figure 8. Sound level distribution at 125 Hz for the standard vertical barrier (NB1), showing diffraction over the barrier top and limited shadow zone at low frequency.

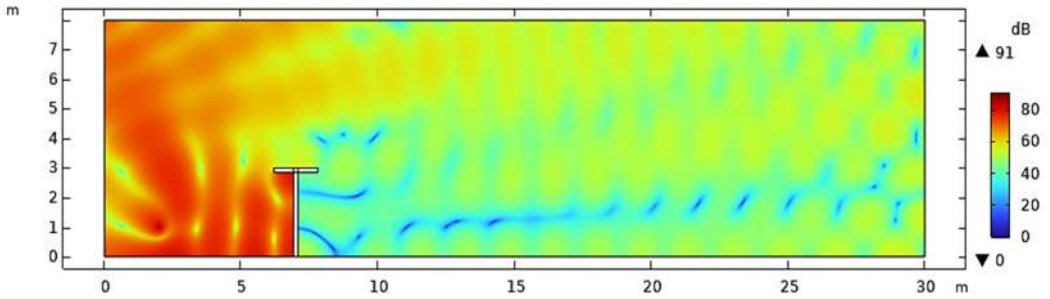


Figure 9. Sound level distribution at 125 Hz for the T-shaped barrier (NB2), where the top edge modifies the diffracted field and slightly enlarges the shadow zone compared to the vertical barrier (NB1).

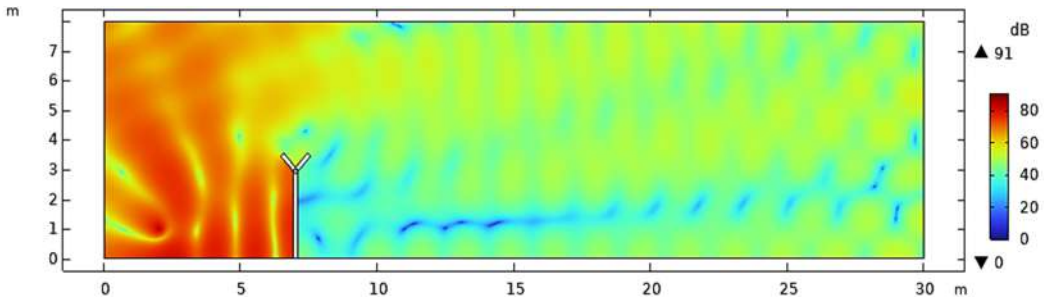


Figure 10. Sound level distribution at 125 Hz for the symmetric V-shaped barrier (NB3), indicating a change in the diffraction pattern at the top edge and a reduction in sound levels behind the barrier.

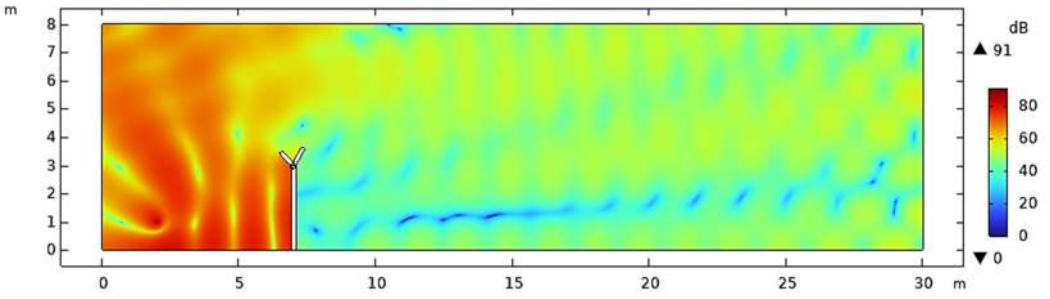


Figure 11. Sound level distribution at 125 Hz for the asymmetric V-shaped barrier (NB4), indicating a change in the diffraction pattern at the top edge and a reduction in sound levels behind the barrier.

Additionally, Figure 18 shows graphs with the distribution of the sound pressure level for all reception points and for all frequencies in the range from 100 Hz to 5000 Hz. Although the optimization procedure was performed up to 3150 Hz, higher frequencies are included to provide a broader perspective, as modern traffic noise often contains significant high-frequency components associated with tire–pavement interactions. In order to enable

a clearer visualization of the results for low frequencies, Figure 19 shows the sound pressure levels only for the frequency range from 100 Hz to 500 Hz.

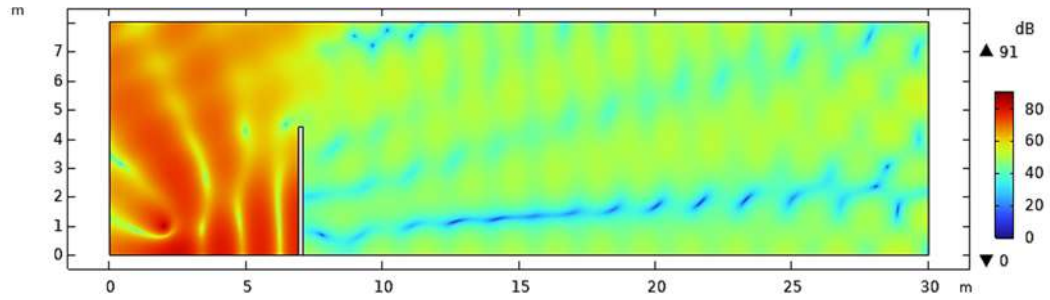


Figure 12. Sound level distribution at 125 Hz for the higher vertical barrier (NB5), showing diffraction over the barrier top and the formation of a shadow zone at low frequency.

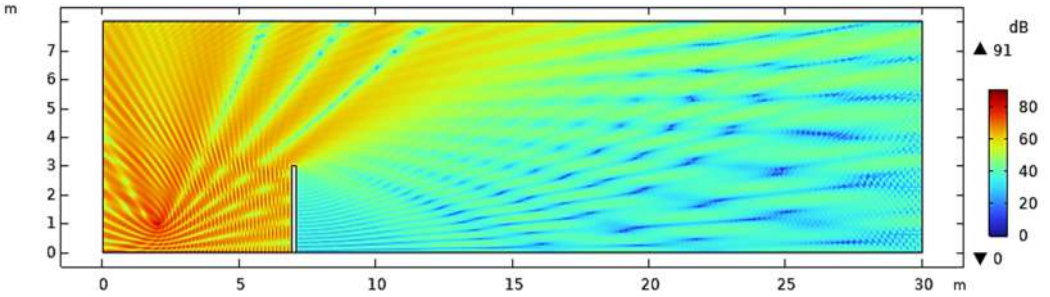


Figure 13. Sound level distribution at 1250 Hz for the standard vertical barrier (NB1), where a more clearly defined shadow zone is formed in the receiver region in comparison to the low-frequency results.

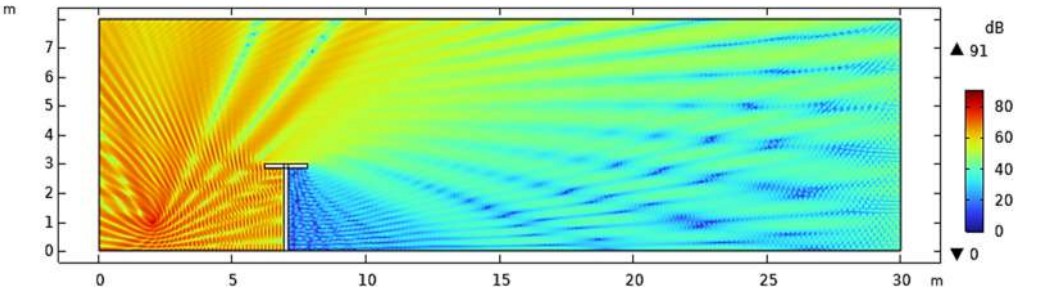


Figure 14. Sound level distribution at 1250 Hz for the T-shaped barrier (NB2), demonstrating improved attenuation in the receiver region due to the influence of the top-edge geometry on diffraction.

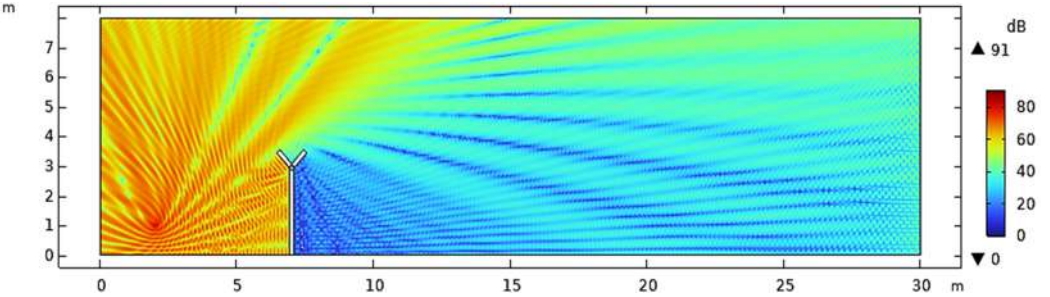


Figure 15. Sound level distribution at 1250 Hz for the symmetric V-shaped barrier (NB3), where the V-shaped termination leads to a strong shadow zone and reduced sound levels behind the barrier.

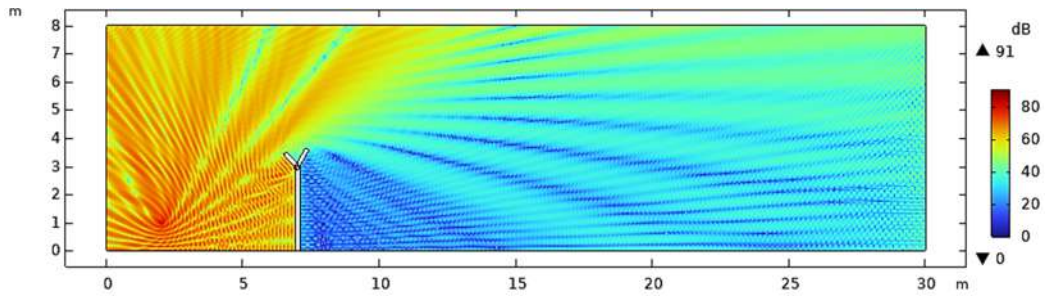


Figure 16. Sound level distribution at 1250 Hz for the asymmetric V-shaped barrier (NB4), where the V-shaped termination leads to a strong shadow zone and reduced sound levels behind the barrier.

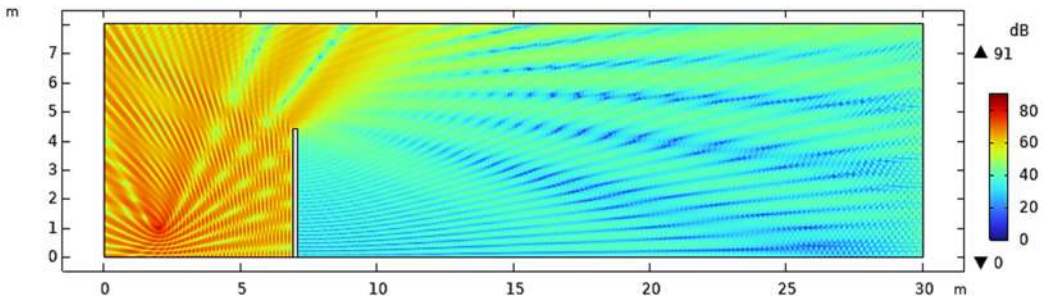


Figure 17. Sound pressure level distribution at 1250 Hz for the higher vertical barrier (NB5), where the increased height improves shielding, although the attenuation remains lower than that achieved by the optimized top-edge configurations.

Based on the results obtained from the optimization process (Table 5), it can be concluded that the best acoustic performance was shown by NB4, i.e., the barrier with an asymmetric V-shaped edge. For this barrier, the value of the objective function was 604.3 dB (as defined by Equation (5)), which is the lowest value. In this barrier, a particularly significant effect was observed at reception point 5, where destructive interference occurs for the frequency of 1600 Hz, resulting in a negative value of the sound pressure level (Figure 18). If zero had been taken instead of a negative value, the corrected value of the objective function would be obtained as 609.4 dB, which again positions this barrier as the most optimal. Barrier NB3, with a symmetrical V-shaped edge, had slightly lower efficiency, with an objective function value of 616.7 dB.

The improved performance of the asymmetric V-shaped termination (NB4) compared with the symmetric V-shape (NB3) can be attributed to the way geometric asymmetry modifies top-edge diffraction and the relationship of the diffracted sound components. In NB4, the unequal slopes and branch lengths lead to phase differences between the diffracted contributions. Consequently, the superposition of contributions from the two edges can increase the likelihood of destructive interference at specific receiver locations and frequencies, which is consistent with the pronounced reduction observed at RP5 around 1600 Hz for NB4.

The most unfavorable result was obtained for NB1 (a standard vertical barrier without an edge, with a height of 3 m), with an objective function value of 687.8 dB, making it the least efficient. The reason for this is the small height and additionally, the absence of a top edge to treat diffraction. The T-shaped edge barrier (NB2) gives better results compared to NB1 (653 dB) even though it has the same height, because the T-edged barrier prevents some of the sound energy from passing through. However, the NB2 barrier is less effective than the NB3, NB4 and NB5 barriers, where the overall height and geometry of the top edges shorten the direct path of sound from the source to the receiver and reduce the effect of diffraction.

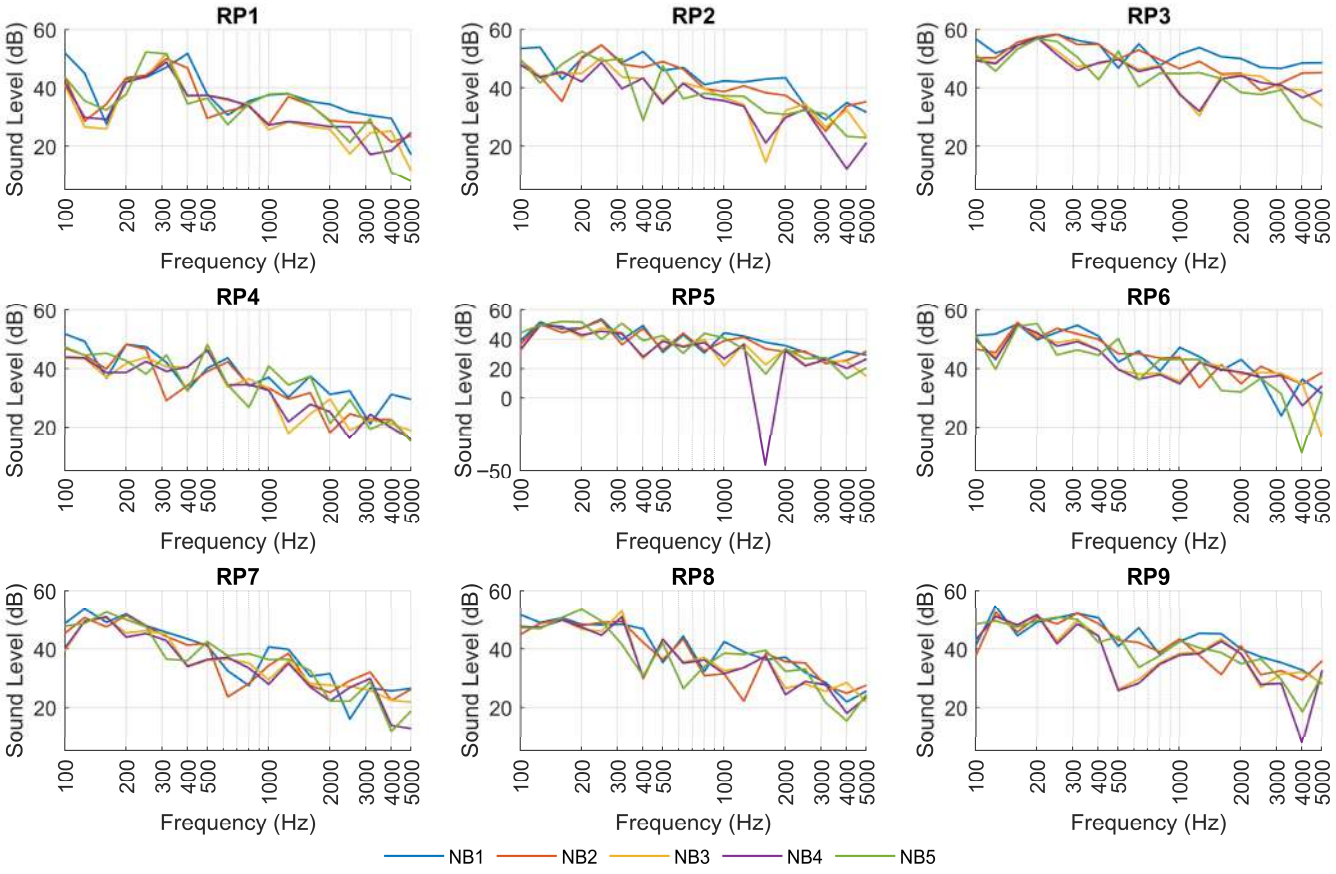


Figure 18. Sound level in reception points (RP) 1–9 in frequency range from 100 Hz to 5000 Hz.

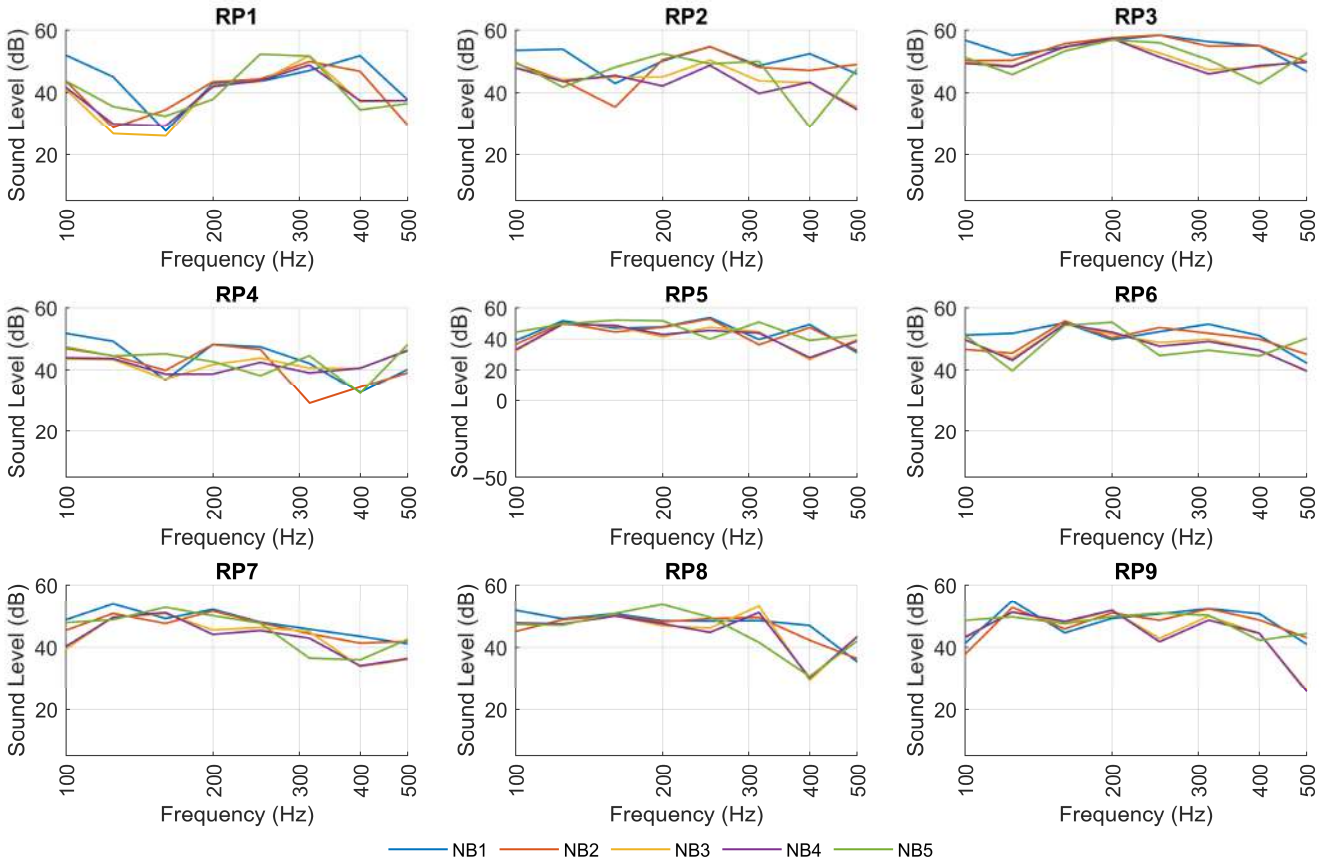


Figure 19. Sound level in reception points 1–9 in frequency range from 100 Hz to 500 Hz.

It is interesting to compare barriers NB3, NB4 and NB5, which have the same volume. NB5, which is a vertical barrier, with height H = 4.4 m, has an objective function of 641.7 dB, which is significantly higher than the objective functions of NB3 and NB4, despite their lower height. This indicates that through appropriate geometric modification of the top edge, better sound efficiency of barriers with the same or lower height can be achieved, which has practical significance for both the esthetics and the economics of the solution.

These conclusions are further supported by the sound field visualizations at 125 Hz and 1250 Hz (Figures 8–17), which show that the barriers with V-shaped top-edge designs produce the most pronounced acoustic shadow zones, particularly at higher frequencies where diffraction effects are more effectively controlled.

Figure 18 shows the sound pressure levels for all reception points for all frequencies. It can be confirmed that the barrier NB1 showed the weakest results. Barrier NB2 with a T-shaped edge performed somewhat better, because the edge prevented the transmission of part of the sound energy. Barriers NB3, NB4 and NB5 had, overall, comparable performance at certain receiving points, where diffraction was not a significant factor. However, at other points, especially for the frequencies 500 Hz and 1000–1250 Hz, NB3 and NB4 show superiority over NB5 by up to 19 dB, despite having a lower height.

Improvements in the low-frequency range are less pronounced than those observed at higher frequencies (Figure 19), where top-edge geometry plays a more dominant role. Within this low-frequency band, barriers NB3 and NB4 exhibit favorable performance. NB5 also shows good attenuation, primarily due to its greater height, whereas NB1 demonstrates the poorest performance.

These frequencies correspond to the dominant energy region of typical road traffic noise. Numerous measurement and modeling studies show that road traffic noise commonly exhibits maximum energy in the mid-frequency range between approximately 500 Hz and 2000 Hz, often with a peak around 1000 Hz [30,31]. The strong performance of the edges in this frequency range therefore highlights their practical relevance for real-world traffic noise mitigation, as they directly target the most acoustically significant part of the traffic noise spectrum.

The results of the present study are consistent with and extend recent research on noise barrier geometry performance and optimization. Similar to the findings of Bugaru et al. [13], the optimized configurations investigated here demonstrate that rigid barriers with modified top-edge geometries are most effective in the mid- to high-frequency range, where diffraction effects govern acoustic shielding. In comparison with the multi-objective optimization study of Toledo et al. [15], which showed that advanced shapes such as polygonal and fork-shaped barriers provide the highest attenuation and that Y-shaped designs outperform tree-shaped and Y-variant configurations, the present work confirms the strong potential of Y-type geometries as efficient and practically realizable alternatives. Furthermore, in agreement with Liu et al. [19], the present results show that T-shaped barriers outperform vertical barriers of the same height; however, this study advances the comparison by additionally considering a vertical barrier with equivalent material volume, for which higher attenuation is obtained. Compared with Sun et al. [9], who reported improved noise reduction for Y-type barriers relative to T-type and vertical barriers, the present study further contributes by systematically evaluating symmetric and asymmetric V-shaped terminations, demonstrating that geometric asymmetry can yield additional performance benefits. Together, these comparisons position the present work as a complementary extension of recent studies.

Future work. The present study focuses on acoustic optimization; however, the practical implementation of optimized reinforced concrete terminations also depends on structural detailing, constructability, and cost. Future investigations should therefore

include an integrated acoustic–structural–economic evaluation, including life-cycle cost analysis, to quantify the trade-off between improved attenuation and potential increases in construction complexity. In particular, asymmetric V-shaped terminations may require more complex formwork and detailing than a standard vertical barrier, which can influence fabrication time, reinforcement layout, and overall cost.

In addition, the traffic noise source was modeled as an idealized line source within a two-dimensional framework. Extending the analysis to three-dimensional models, including finite-length barrier effects and spatially distributed traffic sources, would enable a more realistic representation of actual traffic conditions.

Finally, the incorporation of sound-absorbing treatments represents a further direction for improving barrier performance, particularly at lower frequencies where purely rigid designs are known to be less effective.

4. Conclusions

The analysis of different types of reinforced concrete noise barriers, with and without top edges, showed that the barrier with the V-shaped top edge, particularly the asymmetric variant, offered the highest acoustic efficiency. In particular, the asymmetric V-shaped barrier top edge achieved the lowest value of the objective function, equal to 604.3 (as defined by Equation (5)), compared to 616.7 for the symmetric V-shaped top edge, 653 for the T-shaped top edge, 687.8 for the vertical barrier without a top edge, and 641.7 for the higher vertical barrier with equivalent volume. This improved performance is attributed to the ability of the V-shaped edges to redirect sound energy and reduce diffraction transmission, thus significantly enhancing sound protection.

The optimized barrier with an asymmetric V-shaped edge demonstrated its strongest advantages for the frequencies 500 Hz and 1000–1250 Hz, where pronounced reductions in sound level were observed at specific receiver positions compared to the vertical barrier that has equivalent volume. This frequency range corresponds to the dominant energy content of typical road traffic noise, highlighting the practical relevance of the proposed designs for real-world applications and their potential to effectively reduce human exposure to traffic-related noise.

Geometric optimization emerges as a key element in the modern design of noise barriers, enabling high levels of sound insulation with minimal use of resources. Beyond improving acoustic performance, which is critical for protecting human health, quality of life, and nearby terrestrial and aquatic ecosystems, geometric optimization also contributes to environmentally sustainable design and potential economic benefits by rationalizing material consumption and construction height.

Overall, the results provide meaningful practical guidance for designers, urban planners and engineers in defining effective noise mitigation strategies, particularly in dense urban environments and along heavily trafficked transport corridors.

Author Contributions: Conceptualization, M.J.-M.; Methodology, T.S. and S.B.M.; Software, M.J.-M.; Formal Analysis, T.S.; Investigation, M.J.-M.; Writing—Original Draft, M.J.-M.; Funding Acquisition, S.B.M.; Writing—Review and Editing, T.S. and S.B.M.; Data Curation, T.S. and S.B.M.; Validation, M.J.-M. All authors have read and agreed to the published version of the manuscript.

Funding: This research received no external funding.

Data Availability Statement: Further inquiries can be directed to the corresponding author.

Conflicts of Interest: The authors declare no conflicts of interest.

References

1. European Environment Agency. *Environmental Noise in Europe—2025*; EEA Report No 05/2025; Publications Office of the European Union: Luxembourg, 2025.
2. Environmental Protection Agency. *Guidance Note for Strategic Noise Mapping, Part 1: Requirements for the European Communities (Environmental Noise) Regulations 2018 (As Amended)*; Environmental Protection Agency: Wexford, Ireland, 2025.
3. Münzel, T.; Gori, T.; Babisch, W.; Basner, M. Cardiovascular effects of environmental noise exposure. *Eur. Heart J.* **2014**, *35*, 829–836. [CrossRef] [PubMed]
4. Basner, M.; Babisch, W.; Davis, A.; Brink, M.; Clark, C.; Janssen, S.; Stansfeld, S. Auditory and non-auditory effects of noise on health. *Lancet* **2014**, *383*, 1325–1332. [CrossRef] [PubMed]
5. Shannon, G.; McKenna, M.F.; Angeloni, L.M.; Crooks, K.R.; Fristrup, K.M.; Brown, E.; Warner, K.A.; Nelson, M.D.; White, C.; Briggs, J.; et al. A synthesis of two decades of research documenting the effects of noise on wildlife. *Biol. Rev.* **2015**, *91*, 982–1005. [CrossRef]
6. Holt, D.E.; Johnston, C.E. Traffic noise masks acoustic signals of freshwater stream fish. *Biol. Conserv.* **2015**, *187*, 27–33. [CrossRef]
7. Conference of European Directors of Roads (CEDR). *Technical Report 2017-02: State of the Art in Managing Road Traffic Noise: Noise Barriers*; CEDR: London, UK, 2017. Available online: https://www.cedr.eu/download/Publications/2017/CEDR-TR2017-02-noise-barriers.pdf (accessed on 20 December 2025).
8. Fard, S.M.B.; Kessissoglou, N.; Samuels, S.; Burgess, M. Numerical study of noise barrier designs. In *Proceedings of the Acoustics, Victor Harbor, Australia, 17–20 November 2013*; Australian Acoustical Society: Brisbane, Australia, 2013.
9. Sun, W.; Liu, L.; Yuan, H.; Su, Q. Influence of top shape on noise reduction effect of high-speed railway noise barrier. *IOP Conf. Ser. Mater. Sci. Eng.* **2019**, *493*, 012043. [CrossRef]
10. Monazzam, M.R.; Abbasi, M.; Yazdanirad, S. Performance evaluation of T-shaped noise barriers covered with oblique diffusers using boundary element method. *Arch. Acoust.* **2019**, *44*, 521–531. [CrossRef]
11. Wang, Y.; Jiao, Y.; Chen, Z. Research on the well at the top edge of noise barrier. *Appl. Acoust.* **2018**, *133*, 118–122. [CrossRef]
12. Komkin, A.I.; Musaeva, R.N. Sound level reduction reduction by T-shaped barriers. *Acoust. Phys.* **2023**, *69*, 863–870. [CrossRef]
13. Bugaru, M.; Vasile, O.; Neagoe, M. Recent developments of noise attenuation using acoustic barriers for a specific edge geometry. *Computation* **2021**, *9*, 129. [CrossRef]
14. Liu, H.; Wang, F.; Cheng, S.; Qiu, L.; Gong, Y. Shape optimization of sound barriers using an isogeometric meshless method. *Phys. Fluids* **2024**, *36*, 027116. [CrossRef]
15. Toledo, R.; Aznárez, J.J.; Greiner, D.; Maeso, O. A methodology for the multi-objective shape optimization of thin noise barriers. *Appl. Math. Model.* **2017**, *50*, 656–675. [CrossRef]
16. Ishizuka, T.; Fujiwara, K. Performance of noise barriers with various edge shapes and acoustical conditions. *Appl. Acoust.* **2004**, *65*, 125–141. [CrossRef]
17. Grubeša, S.; Suhanek, M.; Djurek, I.; Petošić, A. Combination of boundary element method and genetic algorithm for optimization of T-shape noise barrier. *Tehnički Vjesnik* **2021**, *28*, 77–81. [CrossRef]
18. Costa, E.G.d.A.; Godinho, L.M.C.; Santiago, J.A.F.; Mansur, W.J.; Peters, F.C. Application of the method of fundamental solutions to predict the acoustic performance of T-shaped thin barriers. *Eng. Anal. Bound. Elem.* **2019**, *99*, 142–156. [CrossRef]
19. Liu, H.; Wang, F.; Zhang, C. Performance analysis and material distribution optimization for sound barriers using a semianalytical meshless method. *Int. J. Mech. Syst. Dyn.* **2023**, *3*, 331–344. [CrossRef]
20. Jolibois, A. A Study on the Acoustic Performance of Tramway Low-Height Noise Barriers: Gradient-Based Numerical Optimization and Experimental Approaches. Doctoral Dissertation, Université Paris-Est, Champs-sur-Marne, France, 2013. Available online: https://theses.hal.science/pastel-00965168v1 (accessed on 31 January 2026).
21. Liu, H.; Wang, F. A novel semi-analytical meshless method for the thickness optimization of porous material distributed on sound barriers. *Appl. Math. Lett.* **2024**, *147*, 108844. [CrossRef]
22. Wang, Y.; Chang, Z.; Chen, G.; Liu, J. Research on the arrangement of additional source for large space protection of an active noise barrier. *Appl. Sci.* **2024**, *14*, 885. [CrossRef]
23. Lee, H.M.; Wang, Z.; Lim, K.M.; Lee, H.P. A review of active noise control applications on noise barrier in three-dimensional/open space: Myths and challenges. *Fluct. Noise Lett.* **2019**, *18*, 1930002. [CrossRef]
24. Iannace, G.; Ciaburro, G.; Trematerra, A. Metamaterials acoustic barrier. *Appl. Acoust.* **2021**, *181*, 108172. [CrossRef]
25. Fan, W.; Cheng, Z.; Xu, S.; Dou, Y. A novel ventilated metamaterial barrier (VMB) for traffic noise reduction. *J. Vib. Eng. Technol.* **2024**, *12*, 4495–4510. [CrossRef]
26. Federal Highway Administration. Noise Barrier Design Handbook—Section 5. U.S. Department of Transportation. Available online: https://www.fhwa.dot.gov/environment/noise/noise_barriers/design_construction/design/design05.cfm (accessed on 31 January 2026).

27. COMSOL Acoustic–Structure Interaction. Frequency Domain. COMSOL Multiphysics® Acoustics Module User's Guide. Available online: https://doc.comsol.com/5.4/doc/com.comsol.help.aco/AcousticsModuleUsersGuide.pdf (accessed on 31 January 2026).
28. COMSOL Perfectly Matched Layers for Pressure Acoustics. COMSOL Multiphysics® Acoustics Module Documentation. Available online: https://doc.comsol.com/6.3/doc/com.comsol.help.aco/aco_ug_pressure.05.139.html (accessed on 31 January 2026).
29. COMSOL The BOBYQA Solver in COMSOL. COMSOL Multiphysics® Acoustics Module Documentation. Available online: https://doc.comsol.com/6.3/doc/com.comsol.help.opt/opt_ug_solver.8.11.html#760988 (accessed on 31 January 2026).
30. Yang, W.; Cai, M.; Luo, P. A road traffic noise spectrum calculation method based on the noise spectral characteristics of single vehicles. In Proceedings of the 48th International Congress and Exposition on Noise Control Engineering (Inter-Noise 2019), Madrid, Spain, 16–19 June 2019.
31. Gjestland, T. *Background Noise Levels in Europe*; Report No. A6631; SINTEF ICT: Trondheim, Norway, 2008. Available online: https://www.easa.europa.eu/sites/default/files/dfu/Background_noise_report.pdf (accessed on 31 January 2026).

Disclaimer/Publisher's Note: The statements, opinions and data contained in all publications are solely those of the individual author(s) and contributor(s) and not of MDPI and/or the editor(s). MDPI and/or the editor(s) disclaim responsibility for any injury to people or property resulting from any ideas, methods, instructions or products referred to in the content.